CrossMark

Processing and electrical properties of gallium-substituted lead zirconate titanate ceramics

Sugato Hajra[1] · Pulkit Sharma[1] · Sushrisangita Sahoo[2] · P. K. Rout[1] · R. N. P. Choudhary[2]

Abstract

In the present paper, the effect of gallium (Ga) substitution on structural, microstructural, electrical conductivity of $Pb(ZrTi)O_3$ (PZT) in the morphotropic phase boundary (MPB) region (i.e., $Pb_{0.96}Ga_{0.04}(Zr_{0.48}Ti_{0.52})_{0.99}O_3$ (PGaZT-4)) was investigated. Increased grain density increases the resistivity of the Ga-modified PZT system. Preliminary structural analysis using X-ray diffraction pattern and data showed the existence of two phases [major tetragonal (T) and minor monoclinic (M)]. Field emission scanning electron micrograph (FESEM) showed the distribution of spherical as well as platelet type grains with small pores. The behavior of dielectric constant with temperature of PGaZT-4 exhibited the suppression of the ferroelectric phase transition [i.e., disappearance of Curie temperature (T_c)]. The complex impedance spectroscopy (CIS) technique helped to investigate the impedance parameters of PGaZT-4 in MPB region in a wide range of temperature (250–500 °C) and frequency (1–1000 kHz) region. The impedance parameters of the material are found to be strongly dependent on frequency of AC electric field and temperature. The substitution of gallium at the Pb site of PZT generally enhances the dielectric constant and decreases loss tangent. The AC conductivity vs frequency ($f = \omega 2\pi$) in the region of dispersion follows the universal response of Jonscher's equation. Enhanced resistive characteristics were observed for Ga-substituted PZT in comparison to the pure PZT, which was well ensured from the studies of electrical parameters, such as impedance and AC conductivity.

1 Background

Among all the ferroelectric oxides known today, lead zirconate titanate (PZT) with varying Zr/Ti ratios have encouraged researchers to design and develop new electronic materials for its enhanced ferroelectric, piezoelectric, pyroelectric properties and electromechanical coupling coefficients. Piezoelectric materials ensure the electromechanical conversion of signal and energy with significantly high piezoelectric effect. This facilitates the chemical substitution very conveniently as compared to the other crystal structure or nearly packed oxygen framework-based perovskite. At high temperatures, it exhibits the perovskite structure of a general formula ABO_3 (A = mono and divalent, B = tri to pentavalent ions) with m3m point group [1]. PZT is a solid–solution of $PbTiO_3$ (ferroelectric, T_c—490 °C) and $PbZrO_3$ (anti-ferroelectric, T_c—230 °C) [2]. The detailed literature survey reveals that 95/5 and 53/47 (Zr/Ti) ratio has two morphotropic phase boundary (MPB) where the structural phase transition occurs from the orthorhombic to rhombohedral system at lower temperatures and rhombohedral to tetragonal at high temperatures, respectively. The phase transitions and material properties of PZT ceramic are strongly affected by domain size. The domain size of the PZT ceramic is dependent on external experimental conditions (temperature), crystal size and defects produced [3]. As MPB is the boundary of two phases, it gives rise to the interesting dielectric and conductive properties. Due to the flexibility in the crystal symmetry and variable chemical compositions, various types of properties of PZT for devices, namely ferroelectric by-pass filter, piezoelectric sensors, transducers, pyroelectric detector, micro-electric motors, memory DRAM, FeRAM and electro-optic application can be tailored [4–8]. Near the MPB, PZT has influenced commercially for its excellent electromechanical and piezoelectric properties of different compositions. Some of these works explored the applications of PZT: Wang et al. [9] used a sono-chemical method for preparation of the

✉ P. K. Rout
  pkrout_india@yahoo.com

1 Department of Electrical and Electronics Engineering, Siksha O Anusandhan University, Bhubaneswar 751030, India

2 Department of Physics, Siksha O Anusandhan University, Bhubaneswar 751030, India

perovskite PZT powder, and investigated the sono-chemical irradiation effects on phase evaluation. Zhou et al. [10] reported the three-thick film technologies for preparation of PZT films used as high-frequency piezoelectric transducers. Smith et al. [11] studied the structural and dielectric properties of nano-structured PZT prepared by self-sustaining polyol auto-combustion method. Kim et al. [12] reported that the ferroelectric properties of the lead titanate ceramic are handled by a flexible substitution at the A-site or the B-site. Tiwari et al. [13] reported the dielectric properties and AC conductivity of $Pb(Zr_{0.65-x}Mn_xTi_{0.35})O_3$ ceramics. Zhang et al. [14] reported that the substitution of lanthanum in PZT enhances the remnant polarization as well as softens the ferroelectric properties. It also lessens the coercive field and useful for the FERAM applications. The addition of dopants may be of two types: acceptor (hard PZT) or donor (soft PZT) [15, 16]. The mobility of the domain and the properties of the modified PZT structure can be controlled by substitution of dopants. In addition, with soft dopants, the piezoelectric properties and relative permittivity are enhanced; as a consequence, the conductivity decreases the transition temperature (T_c). The literature survey suggests that dielectric and spectroscopic studies on Ga-modified PZT (Zr/Ti ratio such as 48/52) have not been done in excess. Panigrahi et al. have already reported the dielectric and electrical properties of PZT with Zr:Ti ratio such as 48:52. They also reported SEM micrograph and piezoelectric coefficient [17]. Buixaderas et al. reported the structural (lattice dynamics, Raman structure) and dielectric properties of soft and hard $PbZr_{0.42}Ti_{0.58}O_3$ [18]. Therefore, we have studied and reported here structural, electrical (conductivity, impedance) and dielectric characteristics (dielectric constant, tangent loss) of 4 weight % Ga-substituted PZT in the MPB region.

2 Methodology

A standard solid-state reaction method was used to prepare PGaZT-4 using high-purity oxides such as PbO, ZrO_2, TiO_2, and Ga_2O_3. These ingredients: lead monoxide (purity-99%, Loba Chemie Pvt. Ltd., India), titanium dioxide (purity-99.5%, Loba Chemie Pvt. Ltd., India), gallium oxide (purity-99.999%, OTTO–Chemika–Biochemica–Reagents, India) and zirconium oxide (purity 99%, Himedia Chemie Pvt. Ltd., India) were weighed by high-precision digital electronic balance (Mettler Toledo PL-E). To compensate the loss occurring during the calcination and sintering, we have taken 2 weight % excess PbO [19]. To achieve proper homogeneous mixture, we have carried out the mixing of ingredients in the air atmosphere for 1 h, and wet atmosphere (methanol) for 1 h keeping it for few times to dry in an agate mortar by slow evaporation. The calcination was

performed in a programmable furnace at 1000 °C for 12 h with a maintained heating rate of 1.7 °C/min. The calcination and sintering processes were carried out in an alumina (Al_2O_3) crucible sealed with Al_2O_3 cover. The dried powder was sieved, and cylindrical pellets (10 mm diameter, 1–2 mm of thickness) were fabricated using a binder (5 weight % of polyvinyl alcohol) and uni-axial pressure of 4×10^6 N/m². The pellets were sintered at a temperature of 970 °C for 10 h in the air atmosphere/open system at the heating rate of 1.6 °C/min. X-ray diffraction pattern (using Bruker diffractometer, model D8 Advance, radiation from CuKα) of prepared samples was recorded with the increment of 0.04° in a wide range of Bragg's angle (θ) ($20° \leqslant 2\theta \leqslant 80°$). The samples were gold-coated and heated for 3 h at a temperature of 150 °C to reduce the effect of PVA binder. The investigation into texture and surface micrograph was done using ZEISS SUPRA 40 field emission scanning electron microscope (FESEM) was carried out. The EDS and elemental mapping were carried out using Oxford Instruments. The silver-painted disks with zero contact resistance were used for dielectric and electrical measurements. The dielectric and electrical parameters were measured with computer-controlled LCR meter (Model: PSM LCR 4NL: 1735, UK) as a function of frequency (1–1000 kHz) at different temperatures (25–500 °C). The LCR meter is pre-configured with a laboratory-fabricated thermocouple coupled with sample holder as well as a heater/furnace. A digital multimeter (Rishabh N25) was utilized to measure the temperature. The frequency- and temperature-dependent dielectric behavior can distinguish between the intrinsic and extrinsic contributions in ferroelectric ceramics. The dielectric responses are dependent on intrinsic (lattice) and external (local defects and phase boundaries) factors [20, 21]. (J–E) curve was measured using a Keithley electrometer at a frequency of 50 Hz.

3 Results and discussion

3.1 Structural and microstructural analysis

In case of polycrystalline material, the randomness of crystal structure allows a fraction of the sample to be oriented with respect to the incident beam which leads to observable arbitrary diffraction lines. With respect to Bragg's law to give d spacing and wavelength, n orders of reflection occur at an angle θ and it is expressed by $2d \sin\theta = n\lambda$ [22]. We need to characterize the composition and microstructure of the newly developed materials with the highest possible manner to understand material behavior.

Figure 1 shows the X-ray diffraction patterns of Ga-modified PZT electronic system. The experimental PGaZT-4 peaks were matched with those of referred XRD
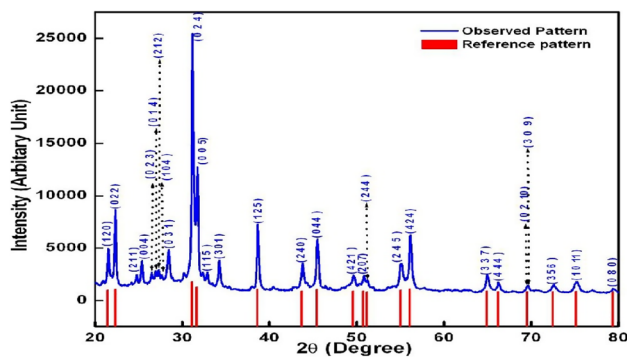
Fig. 1 XRD patterns of PGaZT-4 at room temperature (blue line represents the observed experimental data, red lines is matched with reported PZT peaks)

pattern [23]. It was confirmed through commercially available software "Match Powder Diffraction". The XRD pattern also significantly shows some prominent extra peaks due to the addition of gallium, which clearly highlights two-phase co-existence of two structural systems [tetragonal (T) and monoclinic (M)]. But, the pure PZT sample of same Zr/Ti ratio [17] crystallizes into a single phase compound with tetragonal structure. The reason behind occurrence of these two phases has been investigated by many researchers, but it is still controversial. According to Gibbs phase rule, if there is non-frozen diffusion, then phase diagram lines are replaced by the two-phase coexistence system [24]. The reported work in PZT near MPB also states the presence of two-phase coexistence system (tetragonal and rhombohedral phases vary with composition) was due to meta-stable coexistence; equilibrium coexistence (due to solubility gap), variation in composition (the rate of diffusion of titanium is much greater than the rate of diffusion of zirconium) [25]. This type of behavior may also occur during cooling from the paraelectric to ferroelectric phase transition due to temperature variation [26]. The possible domain numbers of T and M are directly relative to achievement of low-temperature state from the varying state on cooling. The extra monoclinic phase is due to the complex diffraction pattern and internal stress in PGaZT-4, which prevent the calculation of lattice parameters. Past discussion also shows similar existence of monoclinic phase and discussed a diffraction theory of nano-twin super lattices attached to low symmetry phases [27]. Using the Scherer's Eq. [28]: $P = K\lambda/(\beta_{1/2} \cos\theta_{hkl})$ (where $K = $ constant $= 0.89$, $\lambda = 1.5405$ Å and $\beta_{1/2} = $ peak width of the reflection of half intensity) we can determine roughly the crystallite size (P) of PGaZT-4 from the broadening of wide 2θ range peaks. The average value of P was found to be 90 nm. During calculation of crystallite size, we can eliminate the effects of strain and instrument on broadening of peaks.

Figure 2a, b compares the FESEM image of the Ga-free PZT and Ga-modified PZT samples (synthesized in the same environmental conditions) to know the effect of gallium substitution on microstructure. Both the sintering temperature and purity grade of the ingredient oxides have greatly influenced the microstructure of the PGaZT-4 sample. The high-temperature sintering of the pellet and the addition of gallium to Ga-free PZT give rise to an appearance of spherical as well as platelet type of the grains. The surface micrograph of Ga-free PZT (Zr:Ti = 48:52) sample illustrates spherical grains of different sizes with an average grain size in the range of 2–8 μm. It is observed that due to the addition of gallium, there is a non-uniform distribution of spherical and platelet type of grains. The average grain size of both the spherical and platelet grains was calculated for the PGaZT-4 sample. The average grain size of spherical grains is found to be 0.4 μm. The average size of length and breadth of the platelet grains is found to be 2.16 and 0.71 μm, respectively. The induction of plate-like grain in gallium-modified PZT contracts the spherical grains to the reduced size (i.e., from 2 to 0.401 μm) as compared to that of the Ga-free PZT sample. As the platelet grains have been randomly distributed during high-temperature process of the pellet sample, a microstructure with less degree of porosity was obtained. A few large grains observed are the result of agglomeration of a number of smaller grains at higher temperature, stacking faults and planar surface defect [29]. Earlier investigation reported that the size of grains affects the mechanical as well as electrical properties [30]. During the decrease in grain size, the flexural strength and hardness increase significantly [31]. The energy-dispersive X-ray spectroscopy (EDS) helps to study the chemical composition of the prepared material. Detailed analysis of EDS spectra in Fig. 2c shows the presence and homogeneous distribution of lead, zirconium, titanium, gallium and oxygen ions in PGaZT-4 (Table 1). The elemental mapping of the individual element is shown in Fig. 2d.

3.2 Analysis of dielectric parameters

Figure 3a shows the dielectric constant vs temperature plots of PGaZT-4 at various frequencies. Basically, the insulator exhibits dielectric susceptibility and is not temperature sensitive. Ferroelectric materials deviate from this rule. A static dielectric constant varies with temperature according to the Curie–Weiss relation; $\varepsilon_r = B + C/(T - T_c)$ [32], where B and C are temperature-independent constants. C and T_c represent Curie constant and Curie temperature, respectively. For $T > T_c$, the equation holds good. The disappearance (movement of T_c to higher temperature) or suppression of ferroelectric behavior is considered, as the elementary dipoles merge with each other giving rise to an internal field which aligns dipoles. The crystal orientation changed subsequently from noncentro-symmetric to centro-symmetric leading to
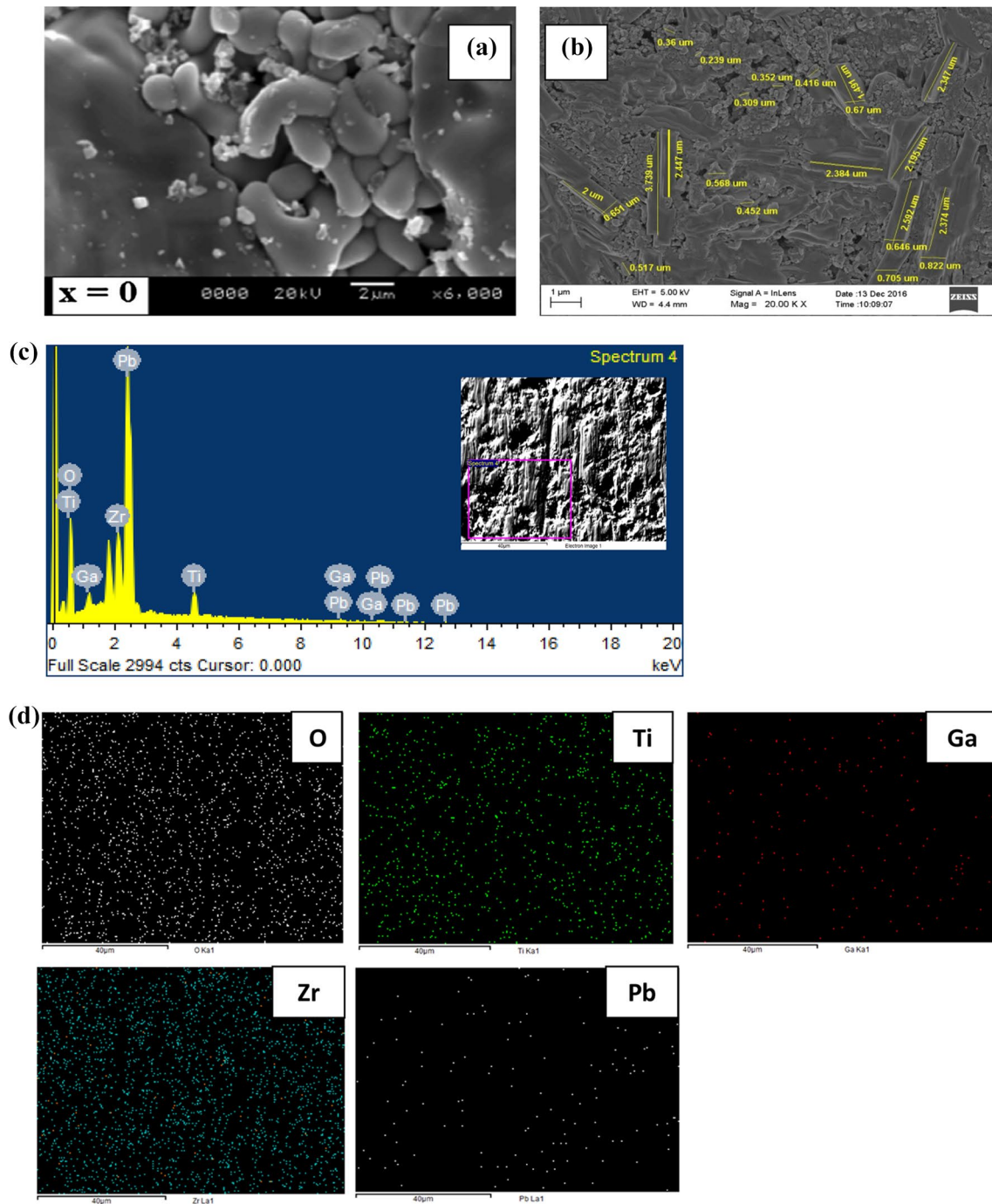
Fig. 2 **a** SEM micrograph of pure PZT and **b** micrograph of gold-coated PGaZT-4 samples. **c** EDS results of PGaZT-4 samples; inset: selected spectrum from the sample surface. **d** Elemental mapping of the PGaZT-4 samples at a marked region. The constituent elements are present all over the surface

such depression. When the temperature is increased, the crystal symmetry is lowered non-typically. Moreover, the non-occurrence of the ferroelectric–paraelectric phase transition is accompanied by the polar–non-polar symmetry change and crystal polarization loss. It may be controversial, but can be restructured by the reconstructive transitional characteristics and by the structural hindrances in the low-temperature phase [33]. As reported earlier [17], the Ga-free PZT sample shows a normal ferroelectric behavior in our studies of temperature-dependent dielectric characteristics of different frequencies. The transition (T_c) is observed at 432 °C at all the given frequencies. The value of dielectric

Table 1 Wt% and At% of PGaZT-4 samples

Element (E)	Wt%	At%
O	33.0	81.9
Ti	3.4	2.8
Ga	0.7	0.4
Zr	11.3	4.9
Pb	51.6	9.9

constant at T_c is found to be 2978 at 10 kHz, which decreases to 2162 at 1000 kHz. But due to the addition of gallium in PZT, the T_c is not observed in the same investigated experimental range. It has been suppressed due to the addition of gallium or moved to higher temperature. The value of dielectric constant was also reduced from 500 to 200 in the same experimental conditions (above) of Ga-modified PZT. In the Ga-free PZT sample, a broad dielectric anomaly at 250 and 350 °C is also observed in the tanδ vs temperature plot. Such a behavior is not observed in the Ga-modified PZT sample.

Figure 3b exhibits the decrease in the dielectric parameters with increasing frequency. It can be seen for gallium-substituted PZT in the low-frequency range, the dielectric constant decreases smoothly, but rapidly on increasing frequency. However, it attains a saturation limit at higher frequency (> 10 kHz). In the low-frequency region, dipolar and space charge polarizations take part to form a high dielectric constant [34]. But at higher frequencies, only the electronic polarization contributes to the permittivity. Therefore, higher frequency-dielectric constant is smaller as compared to that of lower frequency [35]. Further, because of decrease of permittivity on rising frequency, dipoles are unable to follow the exact oscillatory field. It can be seen in the inset

graph that the value of tan δ at room temperature is very low (below 0.2) in the vicinity of frequency of 10^3–10^4Hz. In the low-temperature region, an increasing rate of tan δ in the sintered sample is small, but at higher temperatures, this rate of increase is relatively larger. The fast change in the dissipation factor at elevated temperature is considered due to (1) scattering of temperature-dependent charge carriers and (2) presence of defects created during processing of the sample and (3) unknown impurity phase of the samples.

3.3 Conductivity analysis

Figure 4a, b shows the deviation of AC conductivity (σ_{ac}) with temperature at various frequencies. The variation of AC conductivity (σ_{ac}) with the inverse of absolute temperature provides some interesting properties. The DC conductivity is calculated from the bulk resistance R_b, using the formula $\sigma_{dc} = t/(R_b A)$, where t is the thickness of the sample and A corresponds to the area of the electrode deposited on the sample (Table 1). A progressive rise in AC conductivity pattern is observed with increase in temperature. The temperature dependence of AC conductivity characteristics can be explained using Arrhenius relation: $\sigma = \sigma_o \exp\left(\frac{-E_a}{k_B T}\right)$, where

σ is a constant, k_B is the Boltzmann constant, E_a is the activation energy for conduction [36]. Activation energies are obtained with change in slope over a wide temperature region, but we have presented activation energy only in the high-temperature region (as shown in the figure). The activation energy for PZT has also been calculated using the Arrhenius equation. The calculated activation energy is found to be 0.57 eV at 100 kHz [17] for Ga-free PZT,
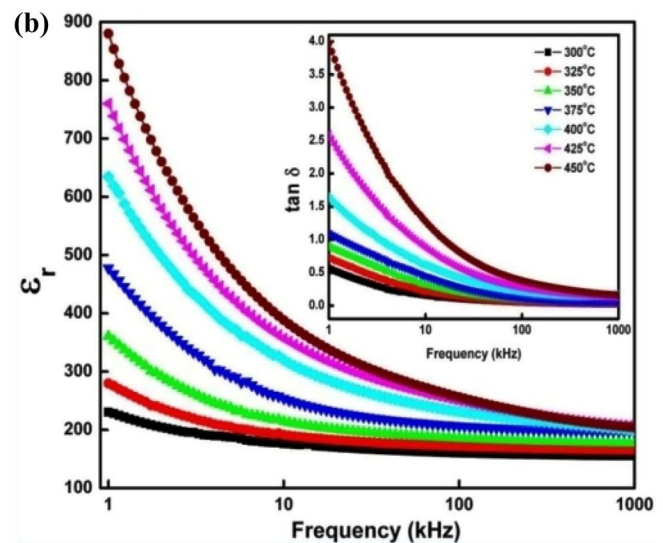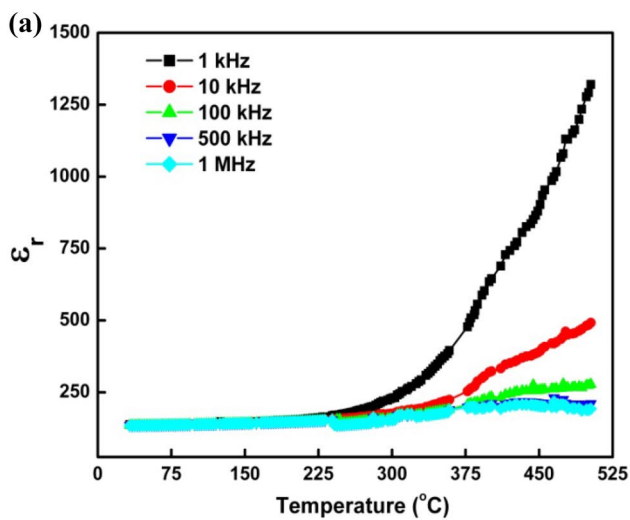

Fig. 3 **a** Temperature-dependent dielectric constant at various frequencies; **b** frequency-dependent dielectric constant; inset: frequency-dependent dielectric loss of PGaZT-4
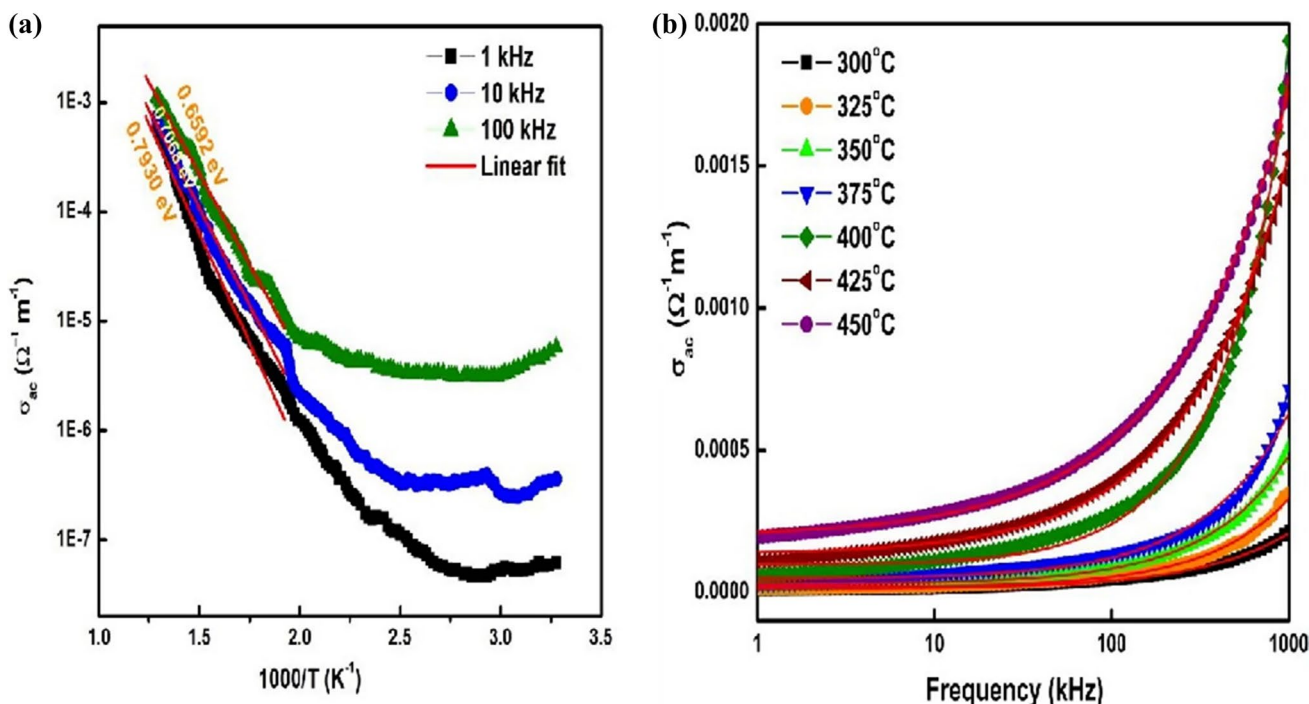
(a)

(b)

Fig. 4 **a** Deviation of AC conductivity vs inverse temperature at frequency, 1 kHz–500 kHz for sample PGaZT-4. **b** Deviation of AC conductivity of sample PGaZT-4 with frequency at different temperatures

whereas this energy for gallium-modified PZT is 0.66 eV. An anomaly (change in slope) is observed in the σ_{ac} vs inverse temperature plot in PZT whereas no such behavior is observed in gallium-modified PZT. The value of AC conductivity for pure PZT increases from 1×10^{-3} to $0.01\ \Omega^{-1}\ m^{-1}$ with a rise in frequency at 450 °C, whereas the value of AC conductivity was found to be reduced from 0.0002 to $0.002\ \Omega^{-1}m^{-1}$ as compared to that of Ga-free PZT. These values of conductivity of PZT and PGaZt-4 suggest the enhancement of resistive characteristics of gallium-modified PZT. The increase in activation energy in Ga-modified PZT may be due to the enhancement in resistive characteristics of the Ga-modified PZT sample in comparison to the Ga-free PZT. There is a linear (frequency independence, i.e., dc field) variation of conductivity at low temperatures, whereas a strong frequency dependence is observed in σ_{ac} vs. frequency spectra. The universal Jonscher's equation ($\sigma_{total} = \sigma_{dc} + A\omega^n$, where symbols have their usual meanings [37]) is used to fit the AC conductivity vs frequency data .

3.4 Impedance analysis

Complex impedance spectroscopy (CIS) technique is commonly used to study structure–properties relationship of a wide variety of materials (ionic insulator, ferroelectric and other related ceramics) in different experimental conditions [38]. In this technique, we apply an alternating

voltage signal to a sample and obtain corresponding phase-shifted current response. The real (´) and imaginary (″) components of the complex (*) electrical parameters such as Z (impedance), modulus (M), and dielectric (ε) can be separated by the CIS technique. Impedance data containing capacitance, resistance and angular frequency can be analyzed using Nyquist plots leading to semicircles. An equivalent circuit with impedance and modulus data collected in different experimental conditions (temperature, frequency) is used to understand a physical process and mechanism of the material. There are three basic formalisms where real and imaginary part of the complex parameters are shown, such as $\varepsilon^* = \varepsilon' - j\varepsilon''$, $Z^* = Z' - jZ''$, $M^* = M' - jM''$ [39].

Figure 5a, b exhibits the frequency variation of Z´ and Z″ at various temperatures. The real and imaginary components of complex impedance can also be written as [40]:

$$Z' = \frac{R}{(1 + \omega\tau)^2},\ Z'' = \frac{\omega R\tau}{1 + (\omega\tau)^2} \tag{1}$$

where R is the resistance, ω is the angular frequency and the relaxation time $= \tau = RC$ (C = capacitance). The nature of variation of these parameters is an indicative of semiconductor behavior of material [41]. However, at higher temperatures and frequencies, semi-conducting properties change to metallic one. The
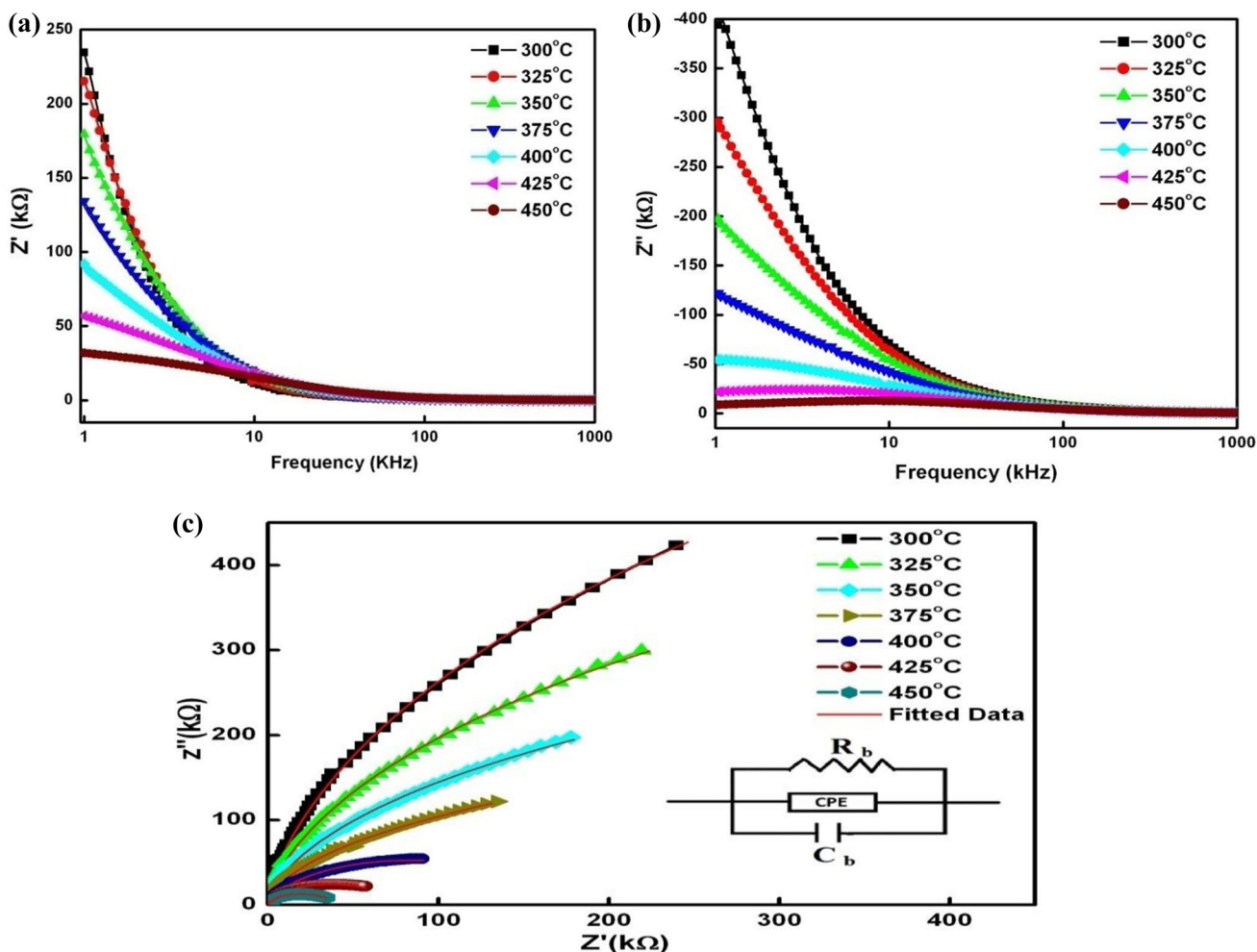
Fig. 5 **a** Variation Z' with frequency for sample PGaZT-4 at different temperatures. **b** Variation Z'' with frequency for sample PGaZT-4 at different temperatures. **c** Variation Z'' with Z' for sample PGaZT-4 at different temperatures

temperature-dependent Z' plots or spectra are merged into a single one above a critical frequency, suggesting the existence and release of space charge [42]. The real part of the impedance generally indicates the resistive nature of the material. It is observed that the value of Z' for Ga-free PZT at low frequency (1 kHz) and high temperature (300 °C) is 110 kΩ [17] whereas for Ga-substituted PZT, it is 240 kΩ. The higher value of Z' suggests that the Ga-modified PZT sample is more resistive as compared to that of Ga-free PZT, which is also observed in conductivity analysis. The peak of the imaginary part of the impedance indicates the existence of dielectric relaxation in the material. Relaxation peaks are observed in the pure PZT sample above 400 °C, which disappeared (not observed) in the Ga-modified PZT sample at that temperature. As mentioned, the vacancies and defects created during material processing and low-temperature immobility of species may be the reasons for occurrence of relaxation process in the material [43].

Figure 5c exhibits Nquist plot (Z' vs Z'' plot or complex impedance plane) which helps to analyze the effect grain, grain boundary and electrode effect from the observed experimental impedance data. But in case of Gallium-doped PZT, at low temperatures the relation between above components is linear which progressively transforms into a circle or semicircle on increasing temperature. The center of the symmetric circle generally falls on the x-axis or below it. If the center of the symmetric semicircular arc falls on the x-axis, dielectric relaxation is considered as a pure Debye type. But, if the center of asymmetric arc is depressed below x-axis (Z' axis), the relaxation process in the material is of non-ideal or non-Debye type [44]. The non-Debye relaxation occurs due to multiple factors such as grain size distribution, grain boundaries, grain orientation and defect distribution [45]. The addition of a constant phase element (CPE) in the model equivalent circuit is required to understand the asymmetry or depressed nature of semicircle [46] in the equivalent circuit model

and electrical response to the material. Additional circuit element CPE provides an ideal capacitor for $n = 1$ and an ideal resistor for $n = 0$. This non-Debye type response can be experimentally as well as theoretically fitted by a software package, ZSIMP WIN Version 2.0 [47, 48]. Depending on the shape of semicircular arc, the various relaxation mechanisms are assigned. The value of bulk conductivity $\sigma_b = t/(R_bA)$ obtained from the complex impedance plots can be considered as true conductivity value, due to negligible thickness of sample surface. The Z' vs Z'' plot helps to determine the value of bulk resistance (R_b); values of bulk capacitance (C_b) and bulk conductivity are shown in Table 2. The parallel combination of capacitance, resistance and a constant phase element was taken as the equivalent circuit to fit the semicircular arcs of the impedance. The interpretation of the electrical behavior of the material is highlighted. The Ga-free as well as Ga-modified PZT

exhibits depressed and asymmetric single semicircular arc indicating only the bulk/grain effect of non-Debye type relaxation. The value of bulk resistance, i.e., R_b decreases from 6.2×10^4 at 400 °C to $2.3 \times 10^4 \Omega$ at 450 °C in Ga-free PZT [17], whereas in Ga-modified PZT the value decreases from 1.875×10^5 to 4.268×10^4 Ω in the same temperature range. Here, we can compare that the value of bulk resistance in Ga-substituted PZT is higher than that of the Ga-free PZT, which again explains the more resistive characteristics of Ga-substituted PZT.

3.5 Electrical modulus study

Figure 6a shows that the small value of M' monotonically increases in the low-frequency region, and thus dispersion occurs with increasing frequency, and subsequently coincided at higher frequencies. The movement of charge carriers of short-range nature and non-Debye type of conduction mechanism are mainly responsible for M′ in the above situation. The flow of charges can be explained by a lack of restoring forces on the application of steady electric field [49].

Figure 6**b** shows that the peak of M'' shifts to the high-frequency region. As the dielectric relaxation process is temperature dependent, relaxation process is related to hopping of charge carriers, thus this process dominates at the higher temperatures only. The existence of non-ideal or non-Debye relaxation was confirmed by asymmetric broadening of M''_{max} peak. It suggests the spreading of relaxation process (thermal relaxation) with different time constants [50].
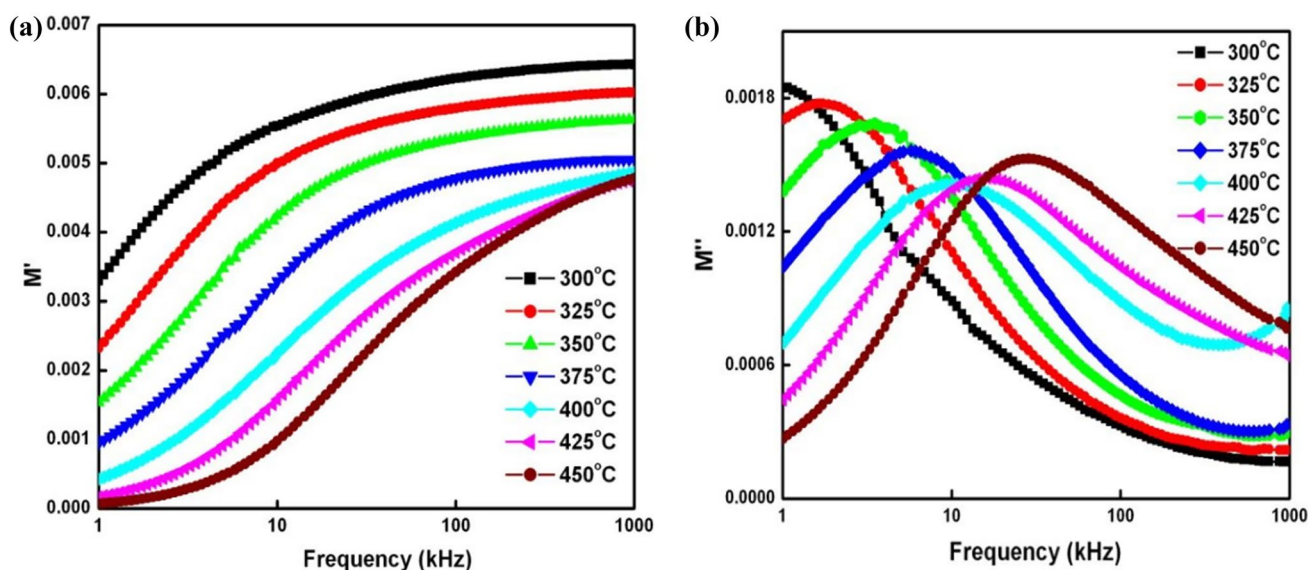
Table 2 Value of grain capacitance (Cg), grain resistance (Rg) and apparent bulk conductivity ($\sigma_{d.c}$) for sample PGaZT-4 at various temperatures

Temperature (°C)	R_g (Ω)	C_g (farad)	$\delta_b = t/(R_b A)$ ($\Omega^{-1}m^{-1}$)
300	2.012×10^6	1.881×10^{-10}	3.5507×10^{-6}
325	2.041×10^6	2.030×10^{-10}	3.5163×10^{-6}
350	3.533×10^6	2.168×10^{-10}	2.0313×10^{-6}
375	7.928×10^6	2.383×10^{-10}	0.9052×10^{-6}
400	1.875×10^5	2.233×10^{-10}	3.8636×10^{-5}
425	8.174×10^4	2.266×10^{-10}	8.7800×10^{-5}
450	4.268×10^4	2.178×10^{-10}	1.6815×10^{-4}

Fig. 6 a Deviation M' with frequency for sample PGaZT at different temperatures. **b** Deviation M'' with frequency for sample PGaZT-4 at different temperatures
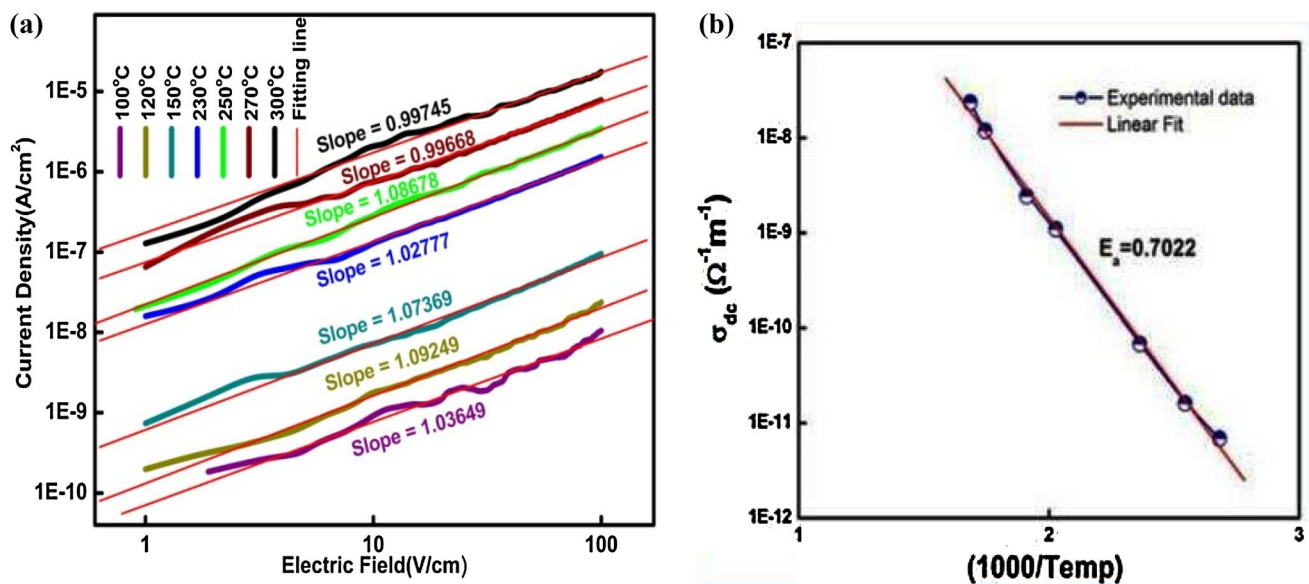
Fig. 7 **a** Current density vs electric field plot and **b** linear fitting of DC conductivity vs temperature

3.6 J–E characterization

Figure 7a indicates the current density (J) with respect to electric field (E) at various temperatures. It is observed that the current density value linearly rises with an increase in the electric field, i.e., shows Ohmic type conduction. The leakage current density is limited by hopping conduction mechanism due to restriction of movement of thermally excited trapped electrons from one site to another [51]. As the conduction mechanism is of Ohmic type, the current density can be expressed as $J = \sigma_{dc} E$. The DC conductivity at various temperatures was found from the slope in Fig. 7b. The plot was well fitted in the form of a straight line and the activation energy was calculated from Arrhenius equation. The temperature-dependent DC conductivity was being observed.

4 Conclusion

PGaZT-4 was prepared by the standard mixed-oxide reaction method. The XRD analysis confirms that two phases coexisting at MPB which was developed due to substitution of gallium at the Pb site of PZT. The Nyquist plots highlighted depressed semicircle which depicts the non-Debye type behavior. The disappearance of T_c or its movement towards high temperature was being observed due to gallium substitution in the PZT. The reduced dielectric loss and less degree of porosity in the microstructure suggest that PGaZT-4 is a low-loss dielectric material. The AC conductivity graph obeys Jonscher's power law, and hence shows a temperature-dependent model in the transport properties

of PGaZT-4 ceramics. From Nyquist plots, the semiconductor nature (negative temperature coefficient of resistance) of the sample is concluded, as the decrease in the growing resistance of the material with the rise in temperatures (positive temperature coefficient of resistance) in some temperate regions is observed. The occurrence of a non-Debye type of relaxation phenomenon in material is confirmed by impedance spectroscopy. The gallium substitution in PZT leads to the formation of the depressed semicircle representing the grain effect. The nature of ions in both localized and non-localized conductions have nearly equal activation energy (as determined from both the Z'' spectra and M'' spectra). Ohmic type of conduction is observed from the current density vs electrical field plot. Hence, these results have distinct advantages such as efficiency, cost effectiveness and flexible dimension which lead to the development of the high-frequency electronics devices and miniaturization of microwave modules.

References

1. C. Duran, S.T. McKinstry, G.L. Messing, J. Electroceram. **10**, 47 (2003)
2. T. Maiti, R. Guo, A.S. Bhalla, Appl. Phys. Lett. **90**, 182901 (2007)
3. G. Arlt, H. Dederichs, R. Herbiet, Ferroelectrics **74**, 37 (1987)
4. I. Naumov, L. Bellaiche, H.X. Fu, Nature **432**, 737 (2004)

5. G. Akcay, S.P. Alpay, G.A. Rossetti, J.F. Scott, J Appl Phys **103**, 024104 (2008)
6. J.F. Scott, Science **315**, 954 (2007)
7. J.F. Scott, C.A.P. Dearaujo, Science **246**, 1400 (1989)
8. G.H. Haertling, J. Am. Ceram. Soc. **86**, 797 (1999)
9. J. Wang, Y. Hu, R. Zhang, L. Song, Z. Chen, Sonochemical preparation of net-lead zirconate titanate (PZT). J. Crystal Growth **263**, 377 (2004)
10. Q. Zhou, S. Lau, D. Wu, K.K. Shung, Prog. Mater. Sci. **56**, 139 (2011)
11. P. Smitha, P.K. Pandey. N.S. Gajbhiye, Polyol based autocombustion synthesis of nanostructured PZT and its characterization. Mater. Chem. Phys **109**, 500 (2008)
12. T. Yong Kim, H.M. Jang, Appl. Phys. Lett. **77**, 3824 (2000)
13. B. Tiwari, R.N.P. Choudhary, Sol. Stat. Sci **11**, 219 (2009)
14. Z. Zhang, P. Wu, L. Lu, C. Shu, Phys. Rev. B **76**, 125102/1 (2007)
15. J. Fousek, V. Janovec, J. Appl. Phys. **40**, 135 (1969)
16. J. Sapriel, Phys. Rev. B **12**, 5128 (1975)
17. S.C. Panigrahi, R. Piyush, B.N. Das, R. Parida, R.N.P. Padhee, Choudhary, J. Alloy. Compd. **604**, 73 (2014)
18. E. Buixaderas, D. Nuzhnyy, P. Vaněk, I. Gregora, J. Petzelt, V. Porokhonskyy, L. Jin, D. Damjanović, Phase Transit. **83**, 917 (2010)
19. S.C. Panigrahi, R. Piyush, B.N. Das, R. Parida, R.N.P. Padhee, Choudhary, J. Mater. Sci. Mater. Electron. **24**, 3275 (2013)
20. D.A. Hall, J. Mater. Sci. **36**, 4575 (2001)
21. Q.M. Zhang, H. Wang, N. Kim, L.E. Cross, J. Appl. Phys. **75**, 454 (1994)
22. S. Niranjan Sahu, Panigrahi, Bull. Mater. Sci **36**, 699 (2013)
23. J. Joseph, T.M. Vimala, V. Sivasubramanian, V.R.K. Murthy, J. Mater. Sci. **35**, 1571 (2000)
24. N. Bassiri-Gharb, Dielectric and piezoelectric non-linearity in oriented Pb(Yb$_{1/2}$Nb$_{1/2}$)O$_3$-PbTiO$_3$ thin films, Doctoral Thesis Dissertation, The Pennsylvania State University, (2005)
25. K. Kakegawa, M. Kawakami, Y. Sasaki, J. Am. Ceram. Soc. **71**, C444 (1988)
26. G.A. Rossetti, A.G. Khachaturyan, G. Akcay, Y. Ni, J Appl Phys **103**, 114113 (2008)
27. Y. Wang, Phys. Rev. B **74**, 104109 (2006)
28. P.K. Sushrisangita Sahoo, R.N.P. Mahapatra, Choudhary, Ceram. Int. **42**, 15955–15967 (2016)

29. H.S. Shulman, M. Testorf, D. Damjanovic, N. Setter, J. Am. Ceram. Soc. **79**, 3124 (1996)
30. S.J. Lee, K.Y. Kang, S.K. Han, Appl. Phys. Lett. **75**, 1784 (1999)
31. N. Ichinose, M. Kimura, Jpn J Appl Phys **30**, 2220 (1991)
32. C. Behera, P.R. Das, R.N.P. Choudhary, J. Electron. Mater. **43**, 3539 (2014)
33. M. Marek Szafran´ski, Jarek, Cryst Eng Comm **15**, 4617 (2013)
34. A.K. Jonscher, Nature **267**, 673 (1977)
35. N. Adhlakha, K.L. Yadav, IEEE Trans. Dielectr. Electr. Insul **2**, 1055 (2014)
36. C.C. Homes, T. Vogt, S.M. Shapiro, S. Wakimoto, A.P. Ramirez, Science **293**, 673 (2001)
37. S. Maity, D. Bhattacharya, S.K. Ray, J. Phys. D Appl. Phys **44**, 095403 (2011)
38. S. Sahoo, P.K. Mahapatra, R.N.P. Choudhary, M.L. Nandagoswami, A. Kumar, Mater. Res. Express **3**, 065017 (2016)
39. R.K. Mishra, R.N.P. Choudhary, A. Banerjee, J. Phys. Condens. Matter. **22**, 025901 (2010)
40. S. Hajra, S. Sahoo, M. De, P.K. Rout, H.S. Tiwari, R.N.P. Choudhary, J Mater Sci Mater Electron, (2017)
41. J. Xia, Q. Zhao, B. Gao, A. Chang, B. Zhang, P. Zhao, R. Maa. J. Alloy. Compd. **617**, 228 (2014)
42. D.K. Pradhan, R.N.P. Choudhary, C. Rinaldi, R.S. Katiyar, J. Appl. Phys. **106**, 024102 (2009)
43. B. Garbarz-Glos, W. Bąk, M. Antonova, M. Pawlik, Mater. Sci. Eng. **49**, 012031 (2013)
44. S. Sahoo, P.K. Mahapatra, R.N.P. Choudhary, J. Phys. D Appl. Phys **49**, 035302 (2016)
45. C.K. Suman, K. Prasad, R.N.P. Choudhary, J. Mater. Sci **41**, 369 (2006)
46. S. Chatterjee, P.K. Mahapatra, R.N.P. Choudhary, A.K. Thakur, Status Solidi **201**, 588 (2004)
47. B.K. Barick, K.K. Mishra, A. K.Arora, R.N.P. Choudhary, D.K. Pradhan, J. Phys. D Appl. Phys. **44**, 355402 (2011)
48. P. Sharma, S. Hajra, S. Sahoo, P.K. Rout, R.N.P. Choudhary, Process. Appl. Ceram. **11**, 171–176 (2017)
49. B.C. Sutar, R. Piyush, R.N.P. Das, Choudhary, Adv. Mat. Lett. **5**, 131 (2014)
50. J.R. Macdonald, Solid State Ionics **13**, 147 (1984)
51. S. Ezhilvalavan, V. Samper, T.W. Seng, X. Junmin, J. Wang, J. Appl. Phys. **96**, 2181 (2004)